Astronomy & Astrophysics manuscript no. photo-z
May 26, 2014

Notes on photo-z for the LSST

J. Cohen-Tanugi, E. Giraud, E. Nuss

Laboratoire Univers et Particules de Montpellier, UMR5299 CNRS-In2p3/Montpellier University, F-34095 Montpellier

ABSTRACT

Context. Deriving redshifts without spectroscopy is a major chalenge of the LSST. We have embarked in the preparation of a dedicated photo-z tool.

Aims. Our first step is to build a set of template spectra and spectral sequences around them. We use a spectroscopic pilot survey in the range $0.3 \leq z \leq 1$, that is reasonably complete up to $R = 23$.

Methods. The spectra are firstly divided in 4 classes, depending on their blue or red SED, absorption or emission lines, and 5 redshift bins from $z = 0.3$ to $z = 1$, measured in the rest frame window 3000 Å - 6000 Å. The stellar mixing and synthetic spectra are derived from the SED using the *starlight* code in that wavelength range, then the model continuum spectra are extended to the range 1000 Å - 10 000 Å.

Results. The 4000 Å break is the main feature in all spectra at all redshifts considered. There are two distinct classes of spectra depending on their general shape above 3000 Å. The first one includes early absorption systems, most of the post-starbursts, red spirals at $z \leq 0.6 - 0.7$, the second one includes blue star-forming galaxies and recent post-starbursts. Among galaxies of the first class the 4300 Å step declines with z around $z = 0.6 - 0.7$ in red spirals, and around $z = 1$ in early ellipticals. All spectra with some recent stellar activity show a clear UV excess between 1500 Å and 2500 Å. Large variations in the UV due to a residual fraction of young stars in early absorption systems or to the age and intensity of the most recent starburst in post-starburst galaxies, may occurr at any look back time. Red emission lines galaxies show an increasing fraction of young stars with z and a decreasing fraction of stars older than ≤ 2.5 Gyr.

Conclusions. The next step is to compare with a spectroscopic atlas. Then we will derive photometric SED, and test our template sequences on photometric surveys with redshifts.

Key words. cosmology - spectral energy distribution - evolution

1. Introduction

In the course of an investigation of the diffuse intergalactic light we obtained galaxy redshifts and spectral flux distributions in a pencil beam of 10' x 10' at magnitude brighter than R = 23 (CDS Catalog; Giraud et al. 2012). Redshift completeness is shown in Figure 1. This pencil beam survey covers a redshift range up to z = 1 (with some galaxies up to z = 1.7). It compares in size with the DEEP1 spectroscopic pilot survey (Weiner et al. 2005). In standard cosmology with $H_o = 75$ km s^{-1} Mpc^{-1}, $\Omega_{0,m} = 0.30$, and $\Omega_{0,\Lambda} = 0.70$, this range provides a large leverage of about 3000 Mpc or 7 Gyr. Our sample was indeed sufficient to extract some of the most conspicuous characteristics on galaxy evolution at $z \leq 1$ (see below).

We will use our pilot survey to prepare a library of spectra covering the main characteristics of galaxy spectra up to z = 1. About half of all stars seem to be still forming, mostly in disks, in this range (Dickinson et al. 2003; Hammer et al. 2005).

Galaxy colors have been shown to segregate in a bimodal distribution (Strateva et al. 2001; Hogg et al. 2002; Blanton et al. 2003) even for field galaxies, corresponding respectively to E, S0, Sa, and Sb, Sc, Irr in the Sloan Digital Sky Survey (SDSS, York et al. 2000). The extensive work on the Cosmic Evolution Survey (COSMOS, Scoville et al. 2007b), confirmed this double distribution between a "red sequence" and a "blue cloud" up to $z = 0.7$ (Cassata et al. 2007, and references therein), a behavior that seems to hold at even higher redshifts ($z \sim 1$, Bell et al. 2004); and up to $z \sim 1.5 - 2$ (Giallongo et al. 2005; Cucciati et al. 2006; Franzetti et al. 2007). Studies based upon extensive data sets (Le Fèvre et al. 2007; Franzetti et al. 2007) have shown that the relative weight of red and blue objects in the bimodal distribution changes with z and environment (Le Fèvre et al. 2007; Franzetti et al. 2007). More precisely, an increase of massive red galaxies with cosmological time was discovered (Bell et al. 2004; Faber et al. 2007, DEEP2 and COMBO-17 data).

More than a decade ago, (Cowie et al. 1996) suggested that while the most massive galaxies were formed early in the Universe, star formation is progressively shifted to smaller systems, the so-called downsizing effect. This effect had been confirmed by several later studies (**?** Bell et al. 2005). This downsizing detected in samples of galaxies at different redshifts has been termed "downsizing in time" to be distinguished from the "archaeological downsizing" which refers to the observation that less massive early type galaxies formed their stellar populations later and over a longer time span than the more massive ones (Thomas et al. 2005; Clemens et al. 2006).

Several studies suggest that the bulk of stars in early-type cluster galaxies had a formation redshift of $z \geq 3$, while those in lower density environments may have formed later, but still at $z \geq 1.5 - 2$ (for reviews see Renzini 2006; Renzini 2007). This may be in contradiction with the rise in the number of massive red galaxies found by Faber et al. (2007) who concluded that most early types galaxies reached their final form below $z = 1$. Our data include a clear red sequence at $z = 0.29$ and a quite large number of absorption systems up to $z \sim 1$ which we fit with population synthesis models in order to search for age variations with z and luminosity.

The main known features of galaxy evolution visible in the pencil beam survey are listed below:

1. Elliptical galaxies. Absorption-line galaxies do not show significant variation in their continuum energy distributions up to $z = 0.6$ and a moderate decrease of the 4000 Å break amplitude of 6% at $z \sim 0.82$, and 15% at $z \sim 1$. Galaxies at $z \geq 0.8$ still had some star formation about 1 Gyr earlier.
2. Archeological downsizing. The faint absorption-line galaxies in our dynamically young cluster at $z = 0.29$ have indexes similar to those of bright absorption-line systems at $z = 0.8$, suggesting that faint galaxies without emission lines tend to be younger than more massive galaxies with similar spectra. Our population synthesis models indicate that 50% of the stars contributing to the spectra of faint absorption-line galaxies at z = 0.29 were formed at $z < 1$. This is consistent with cases of truncated red sequences observed in some high-z clusters and suggests that clusters with truncated red-sequences may be dynamically young. This also suggests that the red sequence is still in a building phase at $z \leq 1$.

3. The average spectra of galaxies with emission lines show significant systematic variations in their energy distribution with z, consistent with what is observed in other regions of the Universe.
4. Downsizing of starbursts. The intrinsic luminosities of starbursts decline with cosmological time, and continue to decrease also in the next evolutionary phase. Therefore, downsizing must take place both in luminosity *and* in number density. In our sample the "down-sizing" phenomenon is of $1.2 - 1.7$ magnitudes from $z = 0.4$ to $z = 0.9$
5. When we divide the sample of emission-line galaxies in two halves by continuum color, we find that the spectral variations are consistent with the following scenario:
   (a) the brightest red emission-line galaxies at $z < 0.5$ have the oldest stellar populations;
   (b) the Universe at $z \leq 0.65$ is repopulated with starburst galaxies at a constant rate down to $z \simeq 0.3$ while at $z \geq 0.65$ the birthrate of starbursts, or the AGN fraction, is higher;
   (c) the red half of emission-line galaxies become redder with decreasing redshift and have lower EQW([OII]) and higher D(4000).
6. The red limit in the energy distribution of emission-line galaxies at $z \leq 0.6$ is typical of bulge-dominated spiral galaxies with moderate star formation, and of early-type LINERs.

The Note is structured as follows. Section 2 describes the survey properties and the method of analysis. The next sections focus on absorption systems, post starbursts, emission lines galaxies with blue and red continuum. Conclusions are in Section 7.

2. Observations and data reduction and survey properties

The observations (ESO program 078A-0456(A) were obtained with the FORS2 instrument (2005) on the Cassegrain focus of the VLT UT1 telescope in multi-object spectroscopy mode with the exchangeable mask unit (MXU). The data reduction, quality of the spectra, and analysis (Giraud et al. 2011) are not repeated here. Figure 1 shows the *R*-magnitude histogram of the galaxies with measured redshifts superimposed on the magnitude histogram of all galaxies in our pencil-beam indicating that our observations sample uniformly at a rate of 50-60% the population of galaxies down to R = 22.5. The sampling seems fairly representative in the magnitude bin R = 22.5 – 23.0, and sparse at R > 23.

Figure 2 presents the magnitude redshift relation and the cone diagrams for the full sample. The points are color coded according to the presence or absence of emission lines.

A cursory inspection of Figure 2 reveals the presence of several conspicuous structures - walls of objects spanning almost the entire field of view - over the full range of redshifts covered by our observations. We see structures centered at $z = 0.29$; two distinct structures at $z \sim 0.4$, which we will denote $z = 0.415$ and $z = 0.447$; a rather complex structure at $z \sim 0.6$, with two main over-densities at $z = 0.58 - 0.63$, and $z = 0.68$; a single rather sparsely populated layer at $z = 0.82$. In what follows, we will refer to these groups as our pencil beam structures. Making bins centered on the peaks of the redshift distribution maximizes the number of objects in each bin and minimizes its redshift dispersion. We combined the spectra in each structure.

The R-band average magnitudes of galaxies in each redshift bin are given in Table 1 separately for absorption, "red" and "blue" emission-line galaxies, together with the distance moduli.

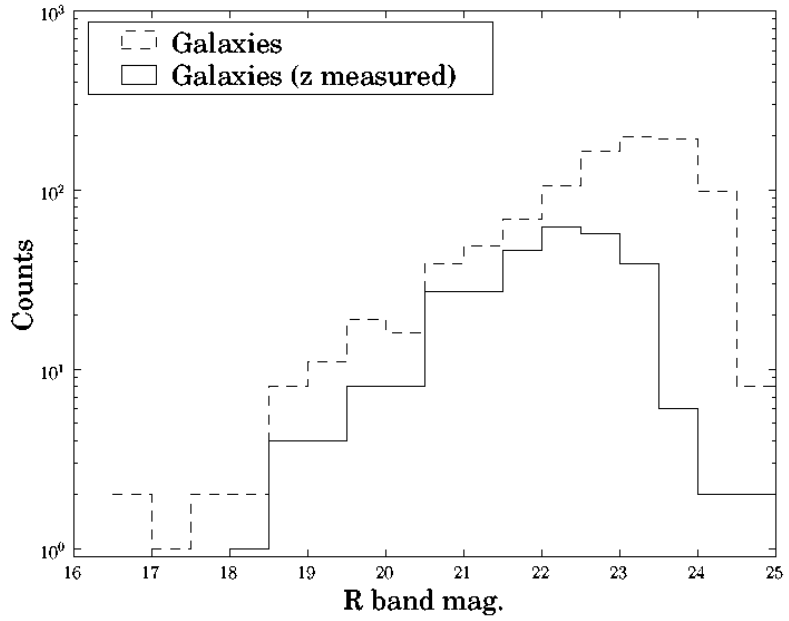

Fig. 1. R-magnitude histogram of galaxies with measured redshift in the central beam.

Table 1. Average R-band magnitudes of absorption systems (abs), and red and blue emission-line galaxies. The adopted distance moduli $(m-M)_0$ and the 4150-4250Å fluxes f normalized to the blue galaxies at $z = 0.9$ are also tabulated.

$< z >$	R(abs)	R(red)	R(blue)	$(m-M)_0$	f(abs)	f(red)	f(blue)
0.29	19.80	20.12	20.97	40.18	0.74	0.72	0.48
0.43	20.24	20.59	20.95	40.86	1.08	0.92	0.75
0.65	21.50	21.60	21.94	41.51	1.42	1.28	0.86
0.9	22.45	22.13	22.35	41.98	2.08	1.70	1

The partition “red” versus “blue” is defined by the median spectral slope in each redshift bin (Section 5.1).

We measured the average fluxes in the wavelength range 4150-4250Å of the galaxies, which we normalized to the flux of blue emission galaxies at $< z >= 0.9$ to compute the luminosity index f. Thus f (that is made equal to 1 for blue galaxies at $< z >= 0.9$) is an indicator of AB(4200) that allows us to compare the luminosities of red and blue galaxies at a given redshift and to investigate luminosity variations with z. Thus Table 1 clearly shows that in each redshift bin, red emission-line galaxies are more luminous than blue galaxies..

2.1. Indexes

The 4000 Å break amplitude and that of 4300 Å step, which are the main continuum features in the observed wavelength range, are given in various tables, together with the [OII] equivalent width.

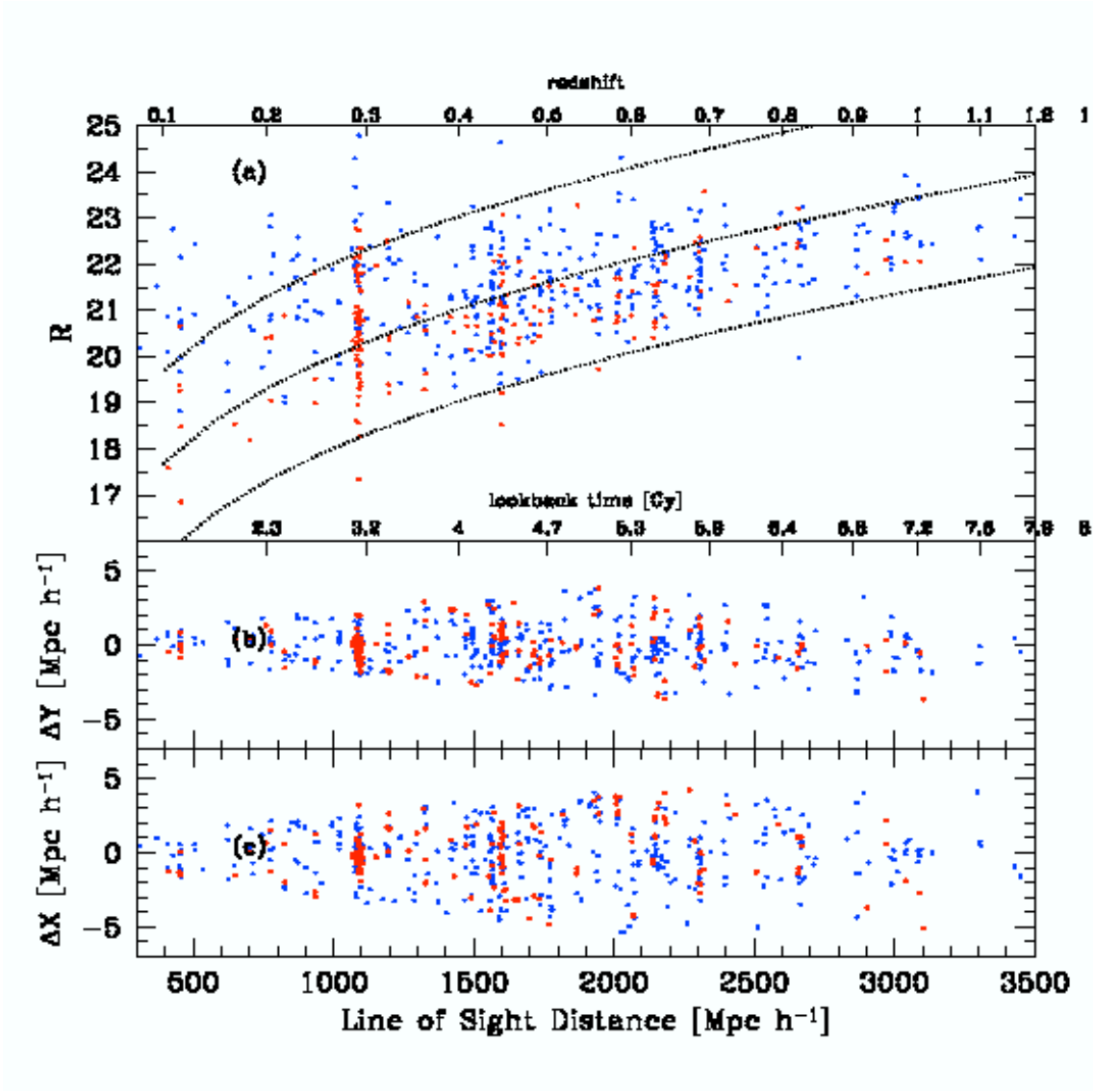

Fig. 2. (a) Magnitude redshift relation for the full sample. The three lines overploted over the measured points correspond to absolute R magnitudes of -22.5, -20.5, and -18.5. The distances have been calculated using a cosmology with $\Omega_{0,\Lambda} = 0.70$, $\Omega_{0,m} = 0.30$, $w = -1$, and $H_0 = 75$km s^{-1} Mpc^{-1} ($h = H_0/75$km s^{-1} Mpc^{-1}). Red dots are galaxies with no emission lines and blue dots are galaxies with emission lines. (b) Cone diagrams in Dec for all the galaxies measured in the field of RX J0054.0-2823. The scales is in Mpc calculated using the angular distance for the standard cosmology. The detection threshold for emission-lines is EQW([OII]) ~ 2 – 3Å. (c) Same as (b) but for RA.

2.2. Stellar Population Analysis

In order to study the stellar population quantitatively, we applied a recent version of the spectral population synthesis code, *starlight*[1] (Cid Fernandes et al. 2004; Gu et al. 2006) to fit the observed and combined spectra. The code does a search for the best-fitting linear combination of 45 simple stellar populations (SSPs), 15 ages, and 3 metallicities (0.2 $Z_\odot$, 1 $Z_\odot$, 2.5 $Z_\odot$) provided

[1] http://www.starlight.ufsc.br/

by (Bruzual & Charlot 2003) to match a given observed spectrum O_λ. The model spectrum M_λ is:

$$M_\lambda(x, M_{\lambda_0}, A_V, v_\star, \sigma_\star) = M_{\lambda_0} \left[\sum_{j=1}^{N_\star} x_j b_{j,\lambda} r_\lambda \right] \otimes G(v_\star, \sigma_\star) \quad (1)$$

where $b_{j,\lambda} = L_\lambda^{SSP}(t_j, Z_j)/L_{\lambda_0}^{SSP}(t_j, Z_j)$ is the spectrum of the j^{th} SSP normalized at λ_0, $r_\lambda = 10^{-0.4(A_\lambda - A_{\lambda_0})}$ is the reddening term, x is the population vector, M_{λ_0} is the synthetic flux at the normalization wavelength, and $G(v_\star, \sigma_\star)$ is the line-of-sight stellar velocity distribution modeled as a Gaussian centered at velocity $v_\star$ and broadened by $\sigma_\star$. The match between model and observed spectra is calculated as $\chi^2(x, M_{\lambda_0}, A_V, v_\star, \sigma_\star) = \sum_{\lambda=1}^{N_\lambda} [(O_\lambda - M_\lambda)\, w_\lambda]^2$, where the weight spectrum w_λ is defined as the inverse of the noise in O_λ. For more details we refer to the paper by (Cid Fernandes et al. 2005).

We rebin the 45 SSPs into 5 components according to age: I ($10^6 \leqslant t < 10^8$ yr), II ($10^8 \leqslant t < 5 \times 10^8$ yr), III ($5 \times 10^8 \leqslant t < 10^9$ yr), IV ($10^9 \leqslant t < 2.5 \times 10^9$ yr), and V ($t \geqslant 2.5 \times 10^9$ yr).

Here we use *starlight* to derive stellar populations models from our spectra in the approximate wavelength range 3000-6000 Å , depending on z. Then we extrapolate the population synthesis spectra to the wavelength range 1000-9000 Å, in order to fit the LSST observing window. The Tables in this Note give the stellar fractions obtained in (Giraud et al. 2011). In the present work we used a more recent stellar library. Figures 4 to 8 are new.

3. Evolution in the pencil beam

The redshift range of our pencil beam survey goes up to $z = 1.72$ with a strong decline above $z \sim 1$. We have truncated the sample at $z = 1.05$. The spectra of all galaxies in five combined redshift bins are shown in Figure 3, where we show the absorption systems (top); and emission line galaxies (bottom), separately. The S/N ratios of the combined spectra are in the range S/N = 22 - 42, for a pixel element of 2.6 Å.

The most conspicuous spectral change with redshift is a decrease in flux redward of the G-band from $< z >= 0.29$ and $< z >= 0.43$ to higher z coupled to an increase to the blue of [OII] from $< z >= 0.65$ to $< z >= 0.82$ and higher z. Since we normalized the spectra at $\lambda\lambda 4050 - 4250$Å, this redistribution of flux is manifested as a rotation of the continuum around a pivot point at $\lambda \sim 4150$Å. This rotation of the normalized spectra implies a systematic change in the galaxy populations entering the sample with redshift: more star forming galaxies at higher z, and more galaxies with old stars at lower z. In order to throw more light on this issue, we fitted simple stellar population (SSP) models to our composite spectra. The results are summarized in Table 3.

4. Absorption line systems

4.1. Absorption systems as function of redshift

The normalized and combined spectra of absorption line systems do not show any obvious change in their continuum and their 4000Å break amplitude up to $z \approx 0.6$ (Table 2). There is a small decrease in the 4000Å break at $z \geq 0.65$ ranging from 5% at $z \sim 0.65$ to 15% at $z \sim 1$ while the Hδ absorption line becomes stronger at $z \geq 0.65$ suggesting the presence of

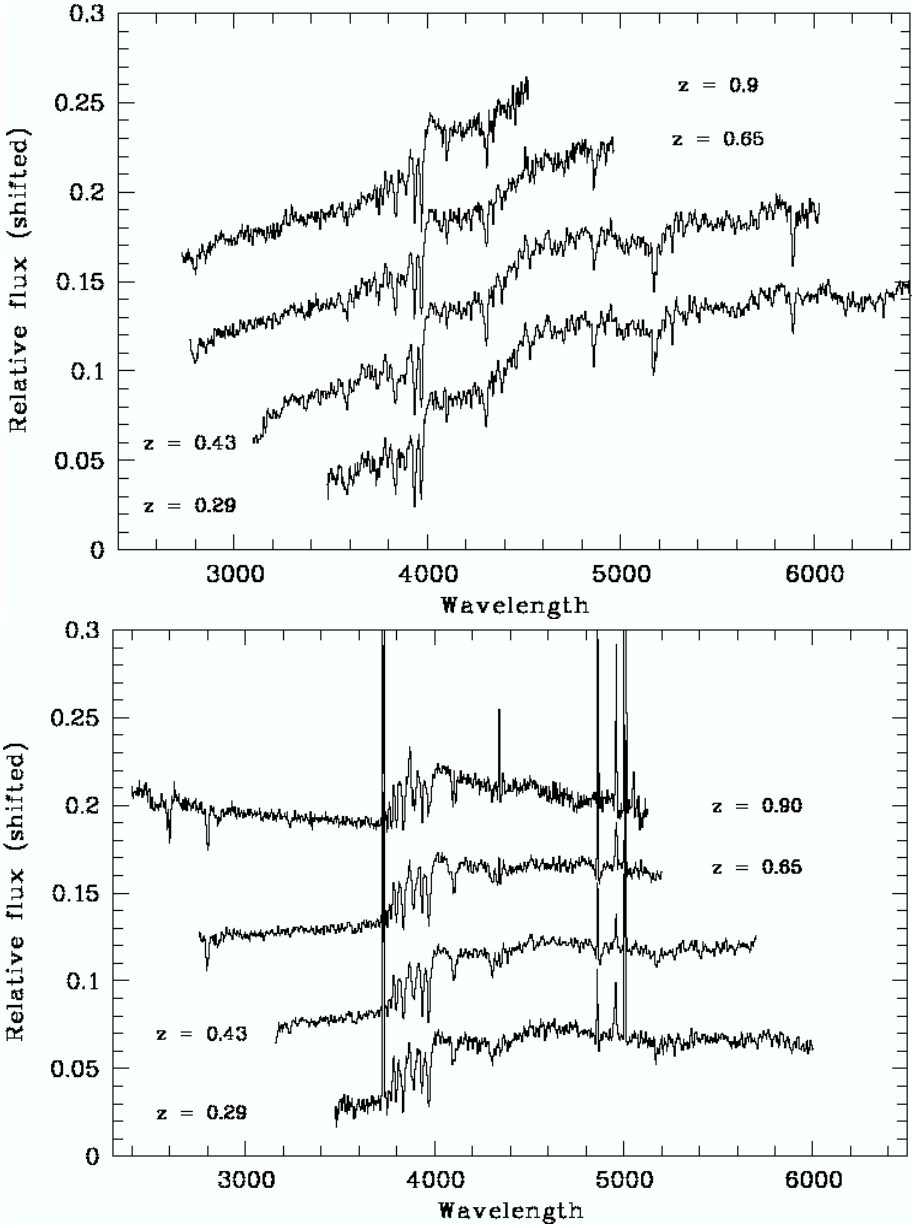

Fig. 3. Composite spectra of absorption systems (top); and emission line galaxies (bottom) normalized in the wavelength range $\triangle\lambda$ = 4050 − 4250 Å. All individual galaxies are brighter than $M_R = -18.8$

Table 2. 4000Å break amplitudes for the full sample, absorption, and emission galaxies. The S/N ratios are those of the combined spectra measured in the wavelength range 4050 - 4250 Å. The magnitude cutoff is $M_R = -18.8$ for all the redshift bins, but is affected by Malmquist bias.

	Full sample		Absorption systems		Emission systems	
< z >	D(4000)	S/N	D(4000)	S/N	D(4000)	S/N
0.29	1.41 ± 0.04	32	1.67 ± 0.065	23	1.22 ± 0.02	32
0.43	1.30 ± 0.03	42	1.70 ± 0.06	22	1.22 ± 0.01	52
0.65	1.24 ± 0.03	38	1.60 ± 0.055	24	1.14 ± 0.01	35
0.82	1.17 ± 0.04	22	1.57 ± 0.06	18	1.07 ± 0.02	28
0.99	1.14 ± 0.04	31	1.43 ± 0.05	23	1.08 ± 0.02	25

Table 3. Stellar population properties of normalized average absorption (abs) and emission (em) spectra in each redshift bin. The magnitude cutoff is at $M_R = -18.8$, except for the 10 faintest absorption systems at $z = 0.29$ where we used all the observed objects.

$< z >$	log(Age):	< 8	$8 - 8.7$	$8.7 - 9$	$9 - 9.4$	> 9.4
0.29	abs	0.0%	0.0%	30.1%	0.1%	69.8%
	abs (10 brightest)	0	0	17.4	0	82.4
	abs (10 faintest)	0	0	12.0	66.4	21.7
	em	16.0	44.1	12.8	1.5	25.7
0.43	abs	0.0	0.7	11.7	6.9	80.7
	em	28.3	14.2	16.5	36.8	4.2
0.65	abs	0.0	0.0	18.2	38.5	43.3
	em	33.1	0.3	65.1	1.4	0.0
0.82	abs	0.0	0.0	86.8	3.3	9.8
	em	21.9	37.1	26.9	0.1	14.1
0.99	abs	0.0	0.0	42.3	0.0	57.7
	em	53.9	9.6	22.7	13.8	0.0

increasing numbers of A stars at higher redshifts. The indexes suggest that these galaxies had the bulk of their star formation at $z \geq 1$, while some of the systems at $z > 0.8$ still had clearly detectable star formation about 1 Gyr ago.

Our SSP models (Table 3) indicate that absorption-line systems at $z \geq 0.65$ show more than 50% of stars younger than 2.5 Gyrs, while those at $z \geq 0.8$ had star formation only about one Gyr ago (Table 3).

The extended synthetic spectra from 1000 to 9000 Å are similar in the wavelength range 3000 - 9000 Å with however a lower 4300 Å step at high z. The models indicate that 80% of the stellar populations in spectra of Figure 4 are older than 1 Gyr except in the spectrum at $z = 1$.

The UV flux variations in absorption spectra below 3000 Å depend on the stellar fraction younger than 500 Myr. Our brightest UV spectra have a tiny fraction ($\leq 2\%$) of stars younger than 100 Myr, the intermediate ones have a detected fraction beteen 100 and 500 Myr, while the lowest ones have no detected stars younger than 500 Myr.

The absorption spectrum at $< z >= 0.99$ has 20% of stars at 500 Myr $\leq$ t $\leq$ 1 Gyr, so it makes a transition with post-starbursts galaxies.

4.2. Post-starbursts

Post-starbursts E+A galaxies are thought to be in a transition phase between a star-forming period and a passively evolving period. Being close to the period of shutdown or quenching of star formation, they probably play an important role in the building of early-type systems (e.g. Wild et al. 2009; Yan et al. 2009). Past studies of intermediate redshift clusters at $0.3 \leq z \leq 0.6$ have found either a higher fraction of post-starbursts in clusters than in the field (Dressler et al. 1999; Tran et al. 2003; Tran et al. 2004), or a similar fraction (Balogh et al. 1999). In fact there is a strong variation in the E+A fraction between the SSDS

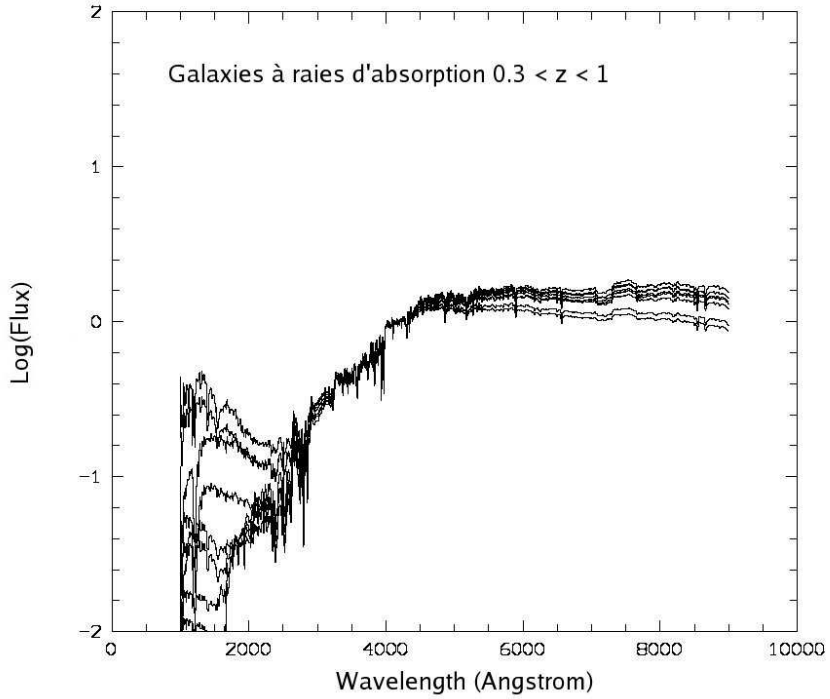

Fig. 4. Spectral synthesis models of absorption systems derived from galaxies in the range $0.3 \leq z \leq 1$, normalized in the wavelength range $4150 - 4250$Å. Flux per Å is in log scale.

low redshift survey at $z \sim 0.07-0.09$, and high z surveys at $z \approx 0.5-1$ (VVDS, Wild et al. 2009), or $z \approx 0.7 - 0.9$ (DEEP2, Yan et al. 2009).

Synthetic spectra of post-starbursts obtained by fitting selected galaxy spectra are shown in Figure 5. They all have strong Balmer absorption lines and have the common property of a large fraction of stars with age 200 Myr $\leq$ t $\leq$ 1 Gyr. They have similar spectra in the visible and huge differences in the UV. Nevertheless they seem to form a sequence which depends on the median age of the burst.

In the top spectrum coloured in blue, with high UV in Figure 5 the starburst occurred at a look back time of 200 Myr. The second spectrum coloured in blue has the average colours of 800 K+A galaxies from the SDSS sample studied by (Melnick & De Propis 2013). Melnick and De Propis used Hα/[NII] for the classification. The oldest stars in these spectra are at 6.2 Gyr. In the spectra coloured in black the peaks are between 500 and 900 Myrs and the oldest stars are at 10 Gyr. The intermediate spectra have peaks at 500 Myrs.

4.3. Absorption systems as function of luminosity at $z = 0.29$

The SSP models indicate that on average about 80% of the stars in the faintest galaxies are younger than 2.5 Gyr (Table 3), i.e. were born at $z < 1$. For comparison, 80% of the stars contributing to the spectrum of the brightest absorption galaxies in the cluster are older than 2.5 Gyr (Table 3).

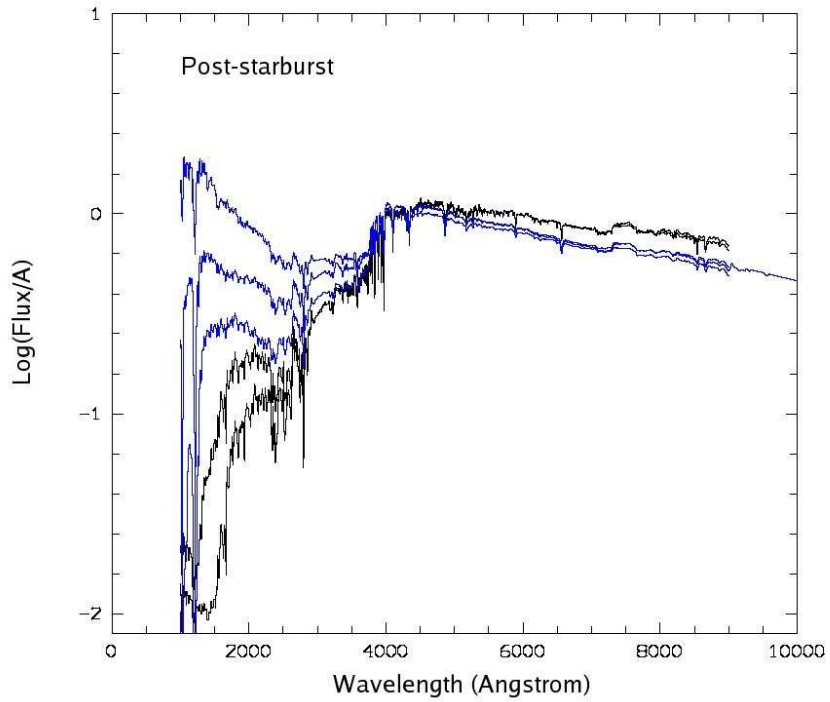

Fig. 5. Spectral synthesis models of post-starburst galaxies obtained by fitting selected galaxy spectra with Starlight.

5. Emission-line galaxies

In the visible range the variation of the spectral continuum of galaxies with emission lines as function of redshift is significantly stronger than that of absorption line systems .

The observed changes in spectral continuum shape in the range $0.3 \leq z \leq 1$, in indexes, and in stellar population models take place over cosmological time scales of order 4 Gyr. Since for single bursts the models predict such variations on time scales of less than 2 Gyr, we interpret the observed spectral changes as an evolutionary sequence where, on average, galaxies with various bursts at various rates and ages, ”migrate” towards redder types as they evolve. These results are in agreement with the well known steep increase in SFR between redshifts 0 and 1 (Pei & Fall 1995; Lilly et al. 1996; Madau et al. 1998; Hopkins & Beacom 2006).

5.1. Partitioning the emission line galaxies in “red” and “blue” systems by their continuum slope

In order to examine the evolution of emission-line galaxies, we partition the sample in two halves: those with continuum slopes bluer than the average and those with continuum slopes redder than the average.

To separate the spectra in to halves, we normalize them in the wavelength range 4150 Å - 4250 Å then we compare their slopes in the range 3600 Å - 6000 Å. The median slope is sample dependant and depends on evolution but it makes sense since the first group contains mostly starburst galaxies and the second objects in a more advanced evolutionary stage. Blue emission lines galaxies have been shown to have higher EQW([OII]) than the red ones.

Table 4. D(4000) and equivalent widths of [OII] and Hδ of average "blue" emission-line galaxies. Values marked (*) have Hδ both in absorption and in emission.

$< z >$	D(4000)	EQW([OII])	EQW(Hδ)	S/N
0.29	1.11 ± 0.01	34.3 ± 0.5	-4 ± 0.5 (*)	23
0.43	1.12 ± 0.01	27.9 ± 0.4	-2.84 ± 0.08	49
0.65	1.09 ± 0.01	30.3 ± 0.7	-5 ± 0.5 (*)	28
0.82	1.04 ± 0.02	53.1 ± 0.8	-6 ± 0.5 (*)	18
0.9	1.02 ± 0.015	53.8 ± 0.8	-5.5 ± 0.5 (*)	23
0.99	1.02 ± 0.02	58.8 ± 0.9	-5 ± 0.5 (*)	12

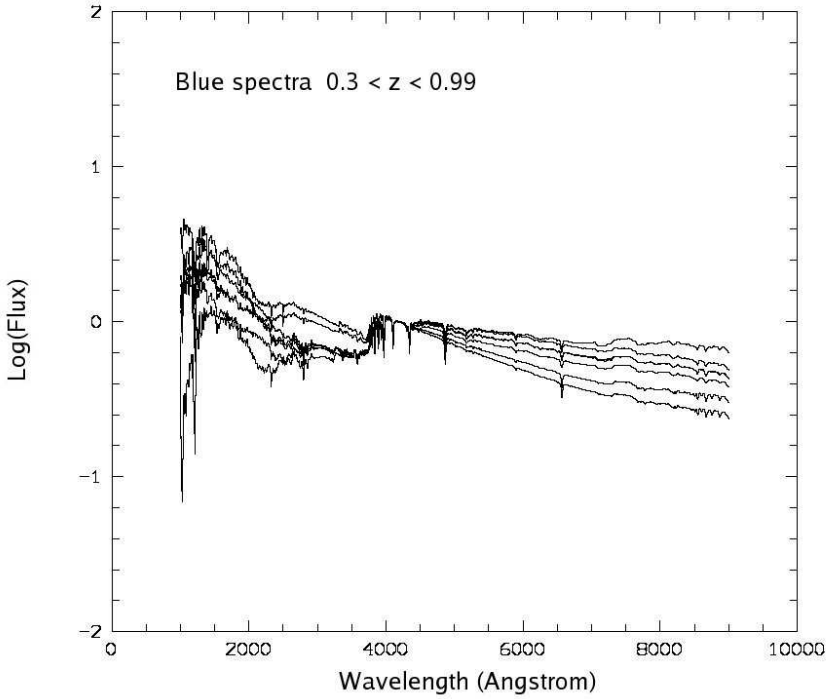

Fig. 6. Spectral synthesis models obtained by fitting spectra of blue emission lines galaxies

5.2. Blue emission line galaxies

The average parameters D(4000), EQW([OII]), and EQW(Hδ) of the spectra obtained by combining the blue half of emission systems are given in Table 4.

5.3. Red emission-line galaxies

After having isolated the two extremes of our galaxy population: starburst dominated emission-line galaxies, and absorption-line systems, we now turn to the galaxies in intermediate evolutionary stages. The most conspicuous changes in the spectra are the systematic increase in UV continuum and [OII] strength with redshift

In order to quantify the evolution of the continuum to the red of the G band, we introduce a G-step index as the ratio of the $[4550-4650]$ Å to the $[4150-4250]$ Å fluxes. The resulting values

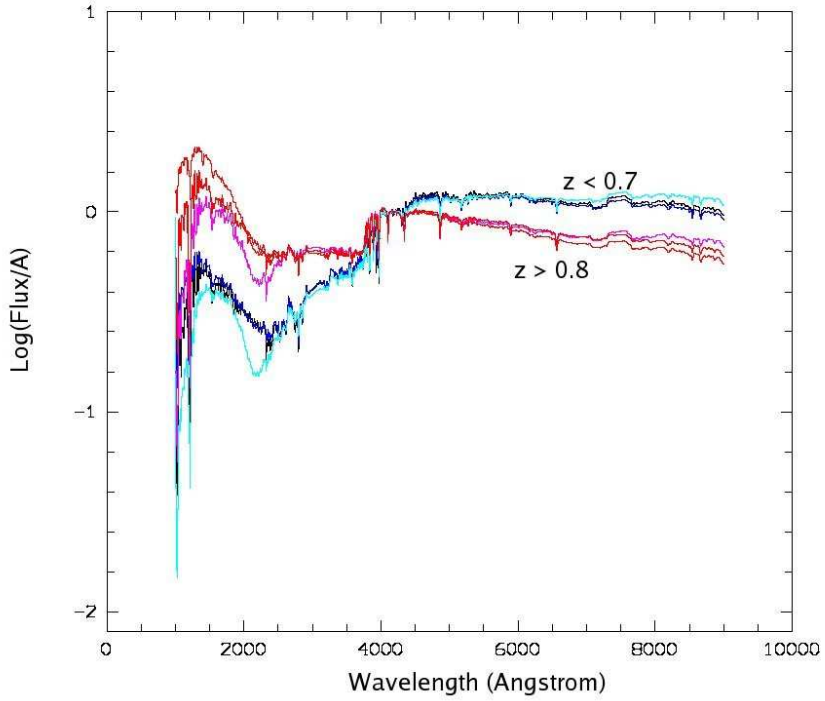

Fig. 7. Spectral synthesis models obtained by fitting spectra of red emission lines galaxies

Table 5. Equivalent widths of [OII] and Hδ in absorption, 4000Å break amplitudes, and G-step indexes for "red" emission systems. The number of galaxies in each bin (N_{gal}) is given in the second column and the dispersions in EQW([OII]) and D(4000) within each bin are given in parenthesis. The values of EQW(Hδ) marked with a (*) are measured as in Table 4. The G-steps of absorption systems are listed in the last column for comparison.

$< z >$	N_{gal}	EQW([OII])	D(4000)	EQW(Hδ)	G step	S/N	G step (abs)
0.29	13	13.2 ± 0.3 (11)	1.324 ± 0.038 (0.53)	−1.89 ± 0.05	1.221 ± 0.012	27	1.470 ± 0.018
0.43	38	10.7 ± 0.5 (4.6)	1.317 ± 0.038 (0.15)	−2.32 ± 0.05	1.164 ± 0.012	34	1.423 ± 0.018
0.65	29	14.3 ± 0.5 (6.0)	1.197 ± 0.037 (0.10)	−4.42 ± 0.05	1.054 ± 0.010	37	1.369 ± 0.017
0.82	11	26.7 ± 0.7 (12.5)	1.118 ± 0.038 (0.08)	−4.6 ± 0.5 (*)	0.977 ± 0.019	22	-
0.9	23	29.5 ± 0.6 (19)	1.132 ± 0.040 (0.09)	−5.3 ± 0.3 (*)	0.971 ± 0.015	25	1.325 ± 0.034
0.99	9	30.3 ± 0.7 (19.7)	1.150 ± 0.050 (0.07)	−5.5 ± 0.5 (*)	0.965 ± 0.020	20	-

are given in Table 5. There is an increase of 16% in the G-step index between $< z >= 0.65$ and $< z >= 0.29$ and a corresponding increase of 9% in the D(4000) break. These variations reach respectively 26% and 15% over the redshift range $< z >= 0.9$ to $< z >= 0.29$. The G-step of absorption systems, also given in Table 5 for comparison, is in all cases larger than the values for the red emission-line galaxies

The SSPs clearly show that star formation in red emission-line galaxies is fading at $z < 0.5$. Extrapoltaing the SSP fits from 1000 Å to 9000 Å clealy shows the decline of the 4300 Å step and the increase of UV flux with z or increasing look-back time (Figure 7). There are large variations in the UV around these median spectra.

Table 6. Stellar population properties of red emission-line galaxies

$< z >$	log Age					χ^2
	< 8	$8 - 8.7$	$8.7 - 9$	$9 - 9.4$	> 9.4	
0.29	0.0	28.3	16.6	25.5	29.5	1.20
0.43	9.0	20.8	30.8	32.7	6.7	0.70
0.65	13.8	25.1	40.9	20.2	0.0	0.68
0.9	18.0	33.2	15.2	33.6	0.0	0.75

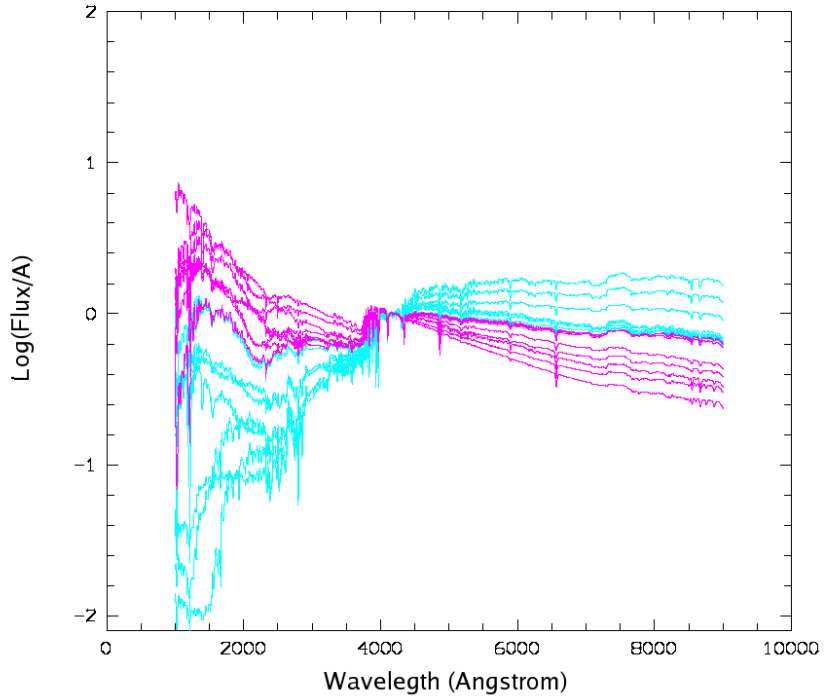

Fig. 8. Continuum spectra divided in two classes by their relative peak amplitude in the UV.

6. Two main classes of spectra?

The main difference in flux spectra measured in normalized SEDs is in the UV where amplitude changes by ~ 2.5dex between low and high relative UV fluxes below 2000 Å. Graphically, there are two main classes of spectra: those with low or high UV which are shown in Figure 8. It may be strange to classify galaxy spectra by the existence of recent bursts that cover short episodes of galaxy lifes, but one may argue that this is not more than recovering the two main classes of stars. Moreover this distinction in two classes may be efficient in a photo-z approach: red spectra, which have no (or weak) UV bump, are those in which the the 4000 Å break is the largest, namely the easiest to detect, while those with a UV bump have a low 4000 Å break amplitude AND a UV bump. In red spectra a photo-z code will search for a step, in blue spectra that will be for a valley. Intermediate spectra will have a detected UV bump and still a quite large break amplitude. This simple approach will be efficient as soon as the peak at 1500 Å enters a ground based UV filter centered at 3500 Å, that is by $z = 1$, and should cover the

"spectroscopic desert" between $z = 1.2$ and $z = 2$. At low z, $g - i$ colour should be discriminant as well.

The red part of our absorption spectra is flatter than that of Gorecki et al's (2104) templates, in particular at larger wavelengths than the 4300 Å step. Our mixing should include more old stars and a different intermediate-to-old age ratio. A similar difference may occurr for red spirals at $z \leq 0.6 - 0.7$. Our blue emission lines form a sequence between Gorecki et al's #3 to #5 spectra. Our post-starburts are also well described by Gorecki et al's red spectra.

7. Summary

We have considered a sample of galaxies spectra in a pencil beam survey at $z \leq 1$ to derive the main features of spectra including those that may change with z.

The 4000 Å break is the only feature in all spectra at all redshifts.

There are two distinct classes of spectra depending on the spectral slope above 3000 Å : 1) Early absorption systems, most of the post-starbursts, red spirals at $z \leq 0.6 - 0.7$ 2) Blue starforming galaxies and recent post-starbursts. Among the first class the 4300 Å step declines with z at about $z = 0.6 - 0.7$ for red spirals, and at about $z = 1$ for ellipticals.

All spectra with some recent stellar activity shows a clear UV excess between 1500 Å and 2500 Å.

Large variations in the UV due to a residual fraction of young stars in early absorption systems or to the age and intensity of the most recent starburst in post-starburst galaxies may occurr at any look back time.

Red emission lines galaxies show an increasing fraction of young stars with z and a decreasing fraction of stars older than ≤ 2.5 Gyr.

In each redshift bin early absorption systems are brighter than red spirals, which in turn are brighter than blue star-forming objects. Starbursts were brighter at large look back time than at low z (Table 1).

Acknowledgements.

References

Balogh, M. L., Morris, S. L., Yee, H. K. C., Carlberg, R. G., & Ellingson, E., 1999, ApJ 527, 54
Bell, E. F., et al, 2004, ApJ 608, 752
Bell, E. F., et al, 2005, ApJ 625, 23
Blanton, M. R., et al, 2003, ApJ 594, 186
Bruzual G., & Charlot S., 2003, MNRAS, 344, 1000
Cassata, P., et al, 2007, ApJS 172, 270
Cid Fernandes R. , et al., 2004, MNRAS, 355, 273
Cid Fernandes R., Mateus A., Sodre L., Stasinska G., Gomes J., 2005, MNRAS 358, 363
Clemens, M.S., Bressan, A., Nikolic, B., Alexander, P., & Rampazzo, R., 2006, MNRAS 370, 702
Cowie, L. L., Songaila, A., Hue, E. M., & Cohen J. G., 1996, AJ 112, 839
Cucciati, O., et al (the VVDS Team), 2006, A&A 458, 39
Dickinson, M., Papovich, C., Fergusson, H.C., Budavari, T., 2003, ApJ 587, 25
Dressler, A., et al., 1999, ApJS 122, 51
Faber, S. et al, 2007, ApJ 665, 265
FORS1+2 User Manual VLT-MAN-ESO-13100-1543 Issue 4, 2005

Franzetti, P., et al (the VVDS Team), 2007, A&A 465, 711
Giallongo, E., et al, 2005, ApJ 622, 116
Giraud, E. et al., 2011 RAA 11, 245
Giraud, E. et al., CDS Catalog 2012, 2012yCatp040001104G
Gorecki, A. et al,. 2014, A&A 561, 128
Gu Q. et al. 2006, MNRAS, 366, 480
Hammer, F., et al, 2005, A&A 430, 115
Hogg, D. W., et al, 2002, AJ 124, 646
Hopkins, A. M., & Beacom, J. F., 2006, ApJ 651, 142
Koyama, Y., Kodama, T., Tanaka, M, Shimasaku, K., & Okamura, S., 2007, MNRAS 382, 1719
Le Fèvre, O. et al, 2007, ASPC 379, 138
Lilly, S. J., Le Fevre, O., Hammer, F., & Crampton, D., 1996, ApJ 460, L1
Madau, P., Pozzeitti, L., & Dickinson, M., 1996, ApJ 498, 106
Melnick, J., & De Propis, R. 2013, MNRAS 431, 2034
Pei, Y. C., & Fall, S. M., 1995, ApJ 454, 69
Renzini, A., 2006, ARA&A 44, 141
Renzini, A., 2007, ASPC 390, 309
Scoville, N., et al, 2007a, ApJS 172, 1
Scoville, N., et al, 2007b, ApJS 172, 150
Strateva, I., et al, 2001, AJ 122, 1861
Thomas, D., Maraston, C., Bender, R., & Mendes de Oliveira, C., 2005, ApJ 621, 673
Tran, K.-V. H., et al, 2007, ApJ 661, 750
Tran, K.-V. H., et al, 2004, ApJ 609, 683
Tran, K.-V. H,. et al, 2003, ApJ 599, 865
Weiner, B.J., et al, 2005, ApJ 620, 595
Wild, V., et al, 2009, MNRAS 395, 144
Yan, R., et al, 2009, MNRAS 398, 735
York, D. G., et al, 2000, AJ 120, 1579